SCIENCE CHINA Materials ARTICLES

mater.scichina.com link.springer.com

Published online 11 May 2018 | https://doi.org/10.1007/s40843-018-9272-3
Sci China Mater 2018, 61(12): 1549–1556

Application of facile solution-processed ternary sulfide Ag_8SnS_6 as light absorber in thin film solar cells

Liangzheng Zhu[1,2], Yafeng Xu[1,2], Haiying Zheng[1,2], Guozhen Liu[1,2], Xiaoxiao Xu[1,2], Xu Pan[1*] and Songyuan Dai[3*]

ABSTRACT **Light absorber is critical to the further applications of thin film solar cells. Here, we report a facile solution-processed method with an annealing temperature below 250°C to fabricate Ag_8SnS_6 (ATS) light absorber for thin film solar cells. After optimization, the ATS-based thin film solar cells exhibited a reproducible power conversion efficiency (PCE) of about 0.25% and an outstanding long-term stability with 90% of the initial PCE retained after a more than 1,000 h degradation test. This research revealed the potential application of ATS as an earth-abundant, low toxic and chemically stable light absorber in thin film solar cells.**

Keywords: thin film solar cells, ternary sulfide, light absorber

INTRODUCTION

Solution-processed thin film solar cells have shown many advanced photovoltaic properties and are considered as promising alternatives to the classic existing photovoltaic technologies [1,2]. In order to minimize the fabrication costs, facile solution processing with low temperature treatment can be an excellent energy-saving option. In addition to the fabrication method, environmentally friendly and earth-abundant material with promising photovoltaic properties is also a key part. However, to date, most of the promising alternatives still cannot meet all the above requirements [3]. Many of them require high energy consumption treatments [4,5] or rely on vacuum deposition [6,7]. Others are limited by containing toxic elements (Pb [8,9], Cd [10,11]) or scarce elements (In [12], Te [13]).

Among the solution-processed thin film solar cells, hybrid organic-inorganic perovskite solar cells (PSCs) are investigated intensively in recent years [14–20], due to the excellent photovoltaic performance of perovskite light absorption materials [21]. Some urgent problems, such as toxic lead content and unstable composition, have hampered outdoor practical applications of PSCs [22–24]. It is an effective way to find potential light absorption materials candidates. Chalcogenides are intensively applied in the photovoltaic field for their variable components and good electronic and optical properties [25,26]. Ternary sulfide Ag_8SnS_6 (ATS) has many excellent photovoltaic properties such as ideal band gap, suitable band edges, high absorption coefficient and remarkable carrier mobility that are comparable with perovskite light absorption materials. ATS has a direct band gap, which is an ideal type for light absorber, because indirect band gap has weak oscillator strengths for both optical absorption and radiative recombination [27]. It means that solar cells based on indirect semiconductors demand a much thicker absorption layer with higher carrier mobility. According to the Shockley-Queisser detailed-balance model, the optimal band gap of a single-junction solar cell is 1.34 eV with a limiting power conversion efficiency (PCE) of 33.7% [28]. Accordingly, the band gap of ATS (1.26 eV) is very close to the ideal band gap. The conduction band edge (CBE) and valence band edge (VBE) are also investigated to make sure that the band positions of ATS are suitable for charge separation. The high coefficient benefited from the direct band gap can mini-

[1] Key Laboratory of Photovoltaic and Energy Conservation Materials, Institute of Applied Technology, Hefei Institutes of Physical Science, Chinese Academy of Sciences, Hefei 230031, China
[2] University of Science and Technology of China, Hefei 230026, China
[3] State Key Laboratory of Alternate Electrical Power System with Renewable Energy Sources, North China Electric Power University, Beijing 102206, China
* Corresponding authors (emails: xpan@rntek.cas.cn (Pan X); sydai@ncepu.edu.cn (Dai S))

mize the thickness of the film [29]. The light absorption coefficient of ATS ranges from 10^4 to 10^5 cm^{-1} distinguished by wavelength, which is in the same order of magnitude reported by literature [30]. The carrier mobility of ATS is in the range of 14–23 cm^2 V^{-1} s^{-1} [31]. Both charge generation and carrier transport can be promoted due to high carrier mobility. Additionally, the weaknesses of $MAPbI_3$ such as toxicity and instability are avoidable in ATS. It is inexpensive, environmentally friendly and chemically stable [32]. As listed above, the talented nature of ATS should make it a promising light absorber.

Several methods for the preparation of ATS micro- and nano-particles have already been reported with their photocatalytic and photoelectric chemical properties [31–34]. However, research about the application of ATS as light absorber in solar cells has been seldom reported. Herein, we presented a novel facile solution-processed method with mild reaction conditions for the fabrication of ATS light absorption layer and successfully applied it in thin film solar cells. The synthesized ATS film presented many good photovoltaic properties. After optimization, ATS-based devices with a reproducible PCE of about 0.25% can be achieved. Meanwhile, the unsealed ATS-based solar cells exhibited a remarkable long-term stability with 90% of the initial PCE retained after 45 days.

EXPERIMENTAL SECTION

Unless stated otherwise, all chemicals were used as received. SnS_2 was synthesized with a method in the literature [35]. $SnCl_4$ (30 mmol, Aldrich) was dissolved in 90 mL of deionized water with constant stirring. Then, ammonium sulfide solution (9.3 mL, Aldrich) was introduced dropwise to the solution to form a yellow precipitation. After centrifugation and washing, yellow precipitate was obtained and then dried in an oven at 80°C. Finally, the precipitate was ground into fine powder.

Sulfur powder (0.2 mmol, SCR), SnS_2 (0.1 mmol) and Ag_2S (0.4 mmol, Alfa Aesar) were introduced in *n*-butylamine (BA) (1 mL, SCR) and thioglycolic acid (TGA) (0.1, 0.2, 0.3 mL, SCR) mixture. Then, the mixed solution was kept at 75°C for 6 h with constant stirring. Finally, a homogeneous black ATS precursor solution was formed. The ATS precursor solution was centrifuged before use.

Fluorine-doped tin oxide (FTO) glass (Pilkington TEC 15) 15 Ω/□ was patterned by etching with Zn powder and 1 mol L^{-1} aqueous HCl. Then, it was cleaned in an ultrasonic bath containing ethanol for 20 min, deionized water for 30 min, and treated at 510°C for 30 min. A dense blocking layer of TiO_2 was deposited on the FTO substrate by aerosol spray pyrolysis at 450°C, using a precursor solution of 0.4 mL of bis-(acetylacetonate) and 0.6 mL of titanium diisopropoxide in 7 mL of isopropanol. TiO_2 (Dyesol 30NRT) paste was diluted in ethanol by mass ratio of 1:3.5. After the FTO substrate was cooled to room temperature, the mesoporous TiO_2 (mp-TiO_2) were deposited by spin-coating the diluted paste at 3,000 rpm. for 20 s and then annealed at 510°C for 30 min. Then, ATS precursor solution was spin-coated on the mesoporous oxide substrate at 4,500 rpm. for 60 s. Subsequently, the film was annealed at 200°C for 30 min in a N_2 atmosphere. A volume of spiro-OMeTAD (2,2',7,7'-tetrakis(*N*,*N*-di-*p*-methoxyphenylamine)-9,9-spirobifluorene, 30 μL) solution was spin-coated on the ATS layer at 4,000 rpm for 30 s. The solution was parepared by mixing 72.3 mg of spiro-OMeTAD, 28.8 μL of 4-*tert*-butylpyridine (TBP), 17.5 μL of lithium bis(trifluoromethylsulphonyl imide (LiTFSI), 520 mg in 1 mL of acetonitrile and 29 μL of tris(2-(1H-pyrazol-1-yl)-4-*tert*-butylpyridine)cobalt(III) bis(trifluoro-methylsulphonyl)imide (FK209), 300 mg in 1 mL of acetonitrile. Finally, the back contact was made by thermally evaporating 60 nm gold on top of the device.

The morphologies of samples were characterized by a field-emission scanning electron microscope (FE-SEM, sirion200, FEI Corp., Holland). The X-ray diffraction (XRD) patterns were measured using a Bruker-AXS Microdiffractometer (model D5005) with Cu Kα radiation (λ=1.5406 Å). Line traces were collected over 2θ values ranging from 10° to 60°. UV-vis absorption spectroscopy and transmittance spectrum were recorded using the UV-vis spectrophotometer (SOLID3700, Shimadzu Co. Ltd, Japan). Ultraviolet photoemission spectroscopy (UPS) were performed on an ESCALAB 250Xi electron spectrometer (Thermo Fisher Scientific) using a monochromatic Al Kα source (300 W). UPS was carried out under a pressure of about 2×10^{-10} Pa using helium Iα (21.22 eV) radiation from a discharge lamp operated at 90 W, a pass energy of 10 eV, and a channel width of 25 meV, and the energy resolution was 0.02 eV. A −9 V bias was applied to the samples, in order to separate the sample and analyze low-kinetic-energy cutoffs. The *J*–*V* curves were carried out *via* a Keithley model 2420 digital source meter controlled by Test point software under a xenon lamp (100 mW cm^{-2}). The irradiance was calibrated using a Si-reference cell certified by NREL. Current-voltage curves were recorded using a sourcemeter (Keithley 2400, USA). All solar cells were covered with a black mask which was

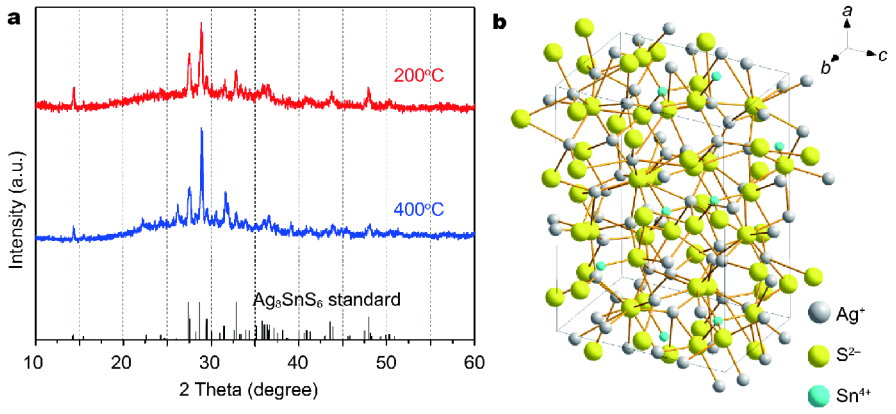

Figure 1 (a) XRD patterns of ATS films synthesized by BA and TGA mixed solvent with different annealing temperature. (b) Crystal structure diagram of ATS.

used to define the active area of the devices, and this case was 0.09 cm^2.

RESULTS AND DISCUSSION

To dissolve sulfide compounds, a mixed solvent of amine and mercapto group can be used [36]. After screening different combinations, two kinds of typical mixtures came in sight: BA/TGA and ethylenediamine (EDA)/2-mercaptoethanol (βME). Although the mixtures of BA/βME and EDA/TGA were also tested, they were not suitable due to poor solubility. Briefly, S, SnS_2 and Ag_2S (2:1:4, molar ratio) were dissolved in BA/TGA (solution A, 1:0.2, *v*/*v*) or EDA/βME (solution B, 1:0.2, *v*/*v*) under stirring at 75°C for 6 h. The introduction of sulfur increases the dissolution of SnS_2 by forming soluble $Sn_2S_6^{2-}$ ions [35]. Black solution A and light yellow solution B can dissolve SnS_2 and Ag_2S. Both solutions were spin-coated on substrates and treated at 200 and 400°C for 30 min, respectively, in N_2 atmosphere. Fig. 1a shows the XRD patterns of Ag-Sn-S compounds synthesized by solution A. It can be concluded that ATS films (PDF#38-0434) with a good crystallinity can be formed by precursor solution A at 200°C. The peak intensity of XRD pattern of the sample treated at 400°C is slightly stronger than that of 200°C, especially for the peaks of (311) lattice planes at 22.6° and (410) at 26.1°. The peaks at 30.47° and 31.97° in the XRD pattern of 400°C are impurity peaks of (101) and (040) lattice planes of SnS (PDF#39-0354). We suppose that a high temperature of 400°C will result in too fast evaporation of solvent and remain unreacted Ag_2S and SnS_2 on the substrate. Solid state Ag_2S and SnS_2 cannot react completely at 400°C and the unreacted SnS_2 decompose into SnS. A previous research also reported the similar phenomenon of SnS_2 decomposed into SnS at 450°C during the solid-phase reaction preparation of ATS [33]. Hence, ATS films should be annealed at 200°C. According to the standard card, the ATS formed after annealing belongs to orthorhombic crystal system, space group $Pna2_1$ (No. 33) with a=15.298 Å, b=7.548 Å and c=10.699 Å. A single ATS unit cell has 4 formula units. S^{2-} anions have two types in the crystal structure (Fig. 1b). One type forms a bond with Ag^+, and the other connects Ag^+ and Sn^{4+} cations together. No obvious characteristic peak assigned to ATS can be observed in the XRD patterns of compounds synthesized by solution B (Fig. S1). This implies that mixed solvent plays an important role and only specific mixed solvents can be functioned in the reactions. As the N−H···S hydrogen bonding formed by amine and mercapto group in the mixture solvent is an important contributor to the dissolving and ionization of metal sulfides [36], we assume that the C=O in TGA can form extensive extra N−H···O hydrogen bonding and this makes the dissolved metal sulfide to have a much higher reactivity. By employing this solution-processed method, stable ATS films with an appropriate crystallinity can be synthesized at a low temperature of 200°C.

Fig. 2a exhibits the UV-vis absorption spectrum of ATS film. The synthesized ATS film has a wide absorption range from the visible light to about 1,000 nm. It proves a narrow band gap of ATS. According to the different synthesis methods and nanoparticle sizes, the band gap of ATS ranges from 1.12 to 1.56 eV in different researches [32,37]. The optical band gap can be calculated by [38]: $(\alpha h\upsilon)=A(h\upsilon-E_g)^n$, where α is absorption coefficient, A is a constant and n is 0.5 or 2 for samples with a direct or indirect band gaps, respectively. The absorption coefficient spectrum of ATS film is presented in Fig. S2. In our cases, the direct band gap (E_g) of ATS is 1.26 eV obtained

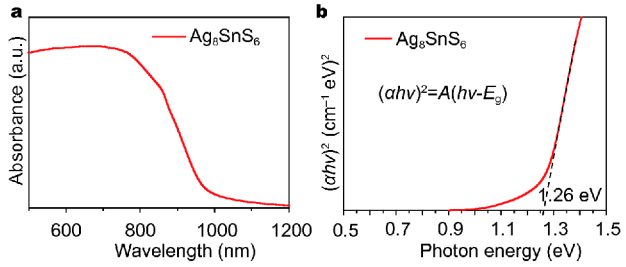

Figure 2 (a) Normalized UV-vis absorption spectrum of ATS film and (b) the corresponding plot of $(\alpha h\nu)^2$ *vs.* $h\nu$ of sample.

by plotting $(\alpha h\nu)^2$ *vs.* $h\nu$ (Fig. 2b). It is a bit smaller than the ideal band gap (1.34 eV) of a single-junction solar cell and could promote a large short current intensity of device.

To further understand the band alignment of ATS, UPS measurement was carried out (Fig. 3a, b). From Fig. 3a, b, the binding energy (E_B) of ATS is 17.2 eV and the VBE is 1.3 eV below the Fermi level. Ionization potential, which can be defined as the energy difference between VBE and vacuum level, is about 5.32 eV. Combined with the band gap, the VBE and CBE of ATS were estimated to be −5.32 and −4.06 eV, respectively (relative to the vacuum level), consistent with the literature [30]. The CBE and VBE of ATS can match well with both conventional electron transport materials (ETM) and hole transport materials (HTM) of thin film solar cells. Fig. 3c shows the schematic diagram of energy levels of each functional layer in ATS thin film solar cells. In our experiments, TiO_2 which has a CBE of −4.20 eV was used as ETM and spiro-OMeTAD with a HOMO level of −5.22 eV was HTM. The ATS light absorption layer was sandwiched between them. This structure is beneficial for the charge separation of ATS absorber, because of the matched energy levels of each layer.

As shown by SEM image in Fig. 4a, the ATS nanoparticles show irregular polygon shapes and the crystallite size ranges from 150 to 400 nm. The atomic force microscopy (AFM) image of ATS is given in Fig. S3 and the R_a of the sample is 52.3 nm. The ATS-based thin film solar cell (FTO/blocking-TiO_2/mp-TiO_2:ATS/ATS/spiro-OMeTAD/Au) was fabricated by a one-step spin-coating method. The thickness of the ATS-based solar cell is about 800 nm (Fig. 4b). The ATS light absorption layer can be divided into two parts. One is the small size ATS nanoparticles which are grown in mesoporous TiO_2 (mp-TiO_2). The other is the large ATS nanoparticles which form a capping layer above the mp-TiO_2:ATS mixture. The mp-TiO_2:ATS mixture layer can increase the contact area between ATS and mp-TiO_2, which will facilitate the electron injection from ATS to mp-TiO_2. The ATS capping layer is designed for sufficient light absorption. When ATS absorbed the incident photons, electrons in the valance band of ATS were excited into the conduction band and left holes in the valance band. These electron-hole pairs were bonded by Coulomb force to form excitons which were separated at the interfaces between ATS and charge transport layers and formed free carriers. These carriers would be injected into charge transport layers under the influence of built-in electric field and then collected and transported by other function layers.

Fig. 5a presents the *J*–*V* curves of typical ATS-based devices made from different volume ratio of mixed solvent. Each group contains 16 samples, and detailed device parameters are shown in Fig. 5b and Table S1. The PCE, short-circuit current density (J_{SC}), open-circuit voltage (V_{OC}) and fill factor (FF) of different BA/TGA mixed solvent based typical devices are 0.22%, 0.67 mA cm^{-2}, 0.62 V and 0.53 for the ratio of 1:0.1 (group α); 0.26%, 0.90 mA cm^{-2}, 0.59 V and 0.49 for the ratio of 1:0.2 (group β); 0.037%, 0.28 mA cm^{-2}, 0.44 V and 0.30 for the ratio of 1:0.3 (group γ), respectively. Group β showed the best PCE, while the PCE of group α was a bit lower. It was mainly attributed to the low J_{SC} of group α. TGA in the

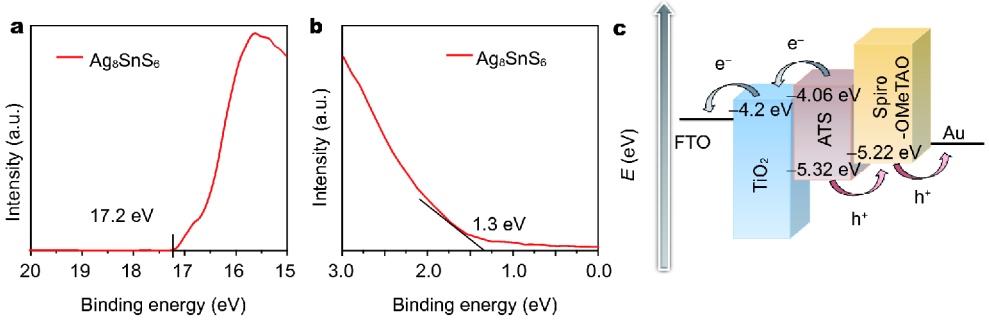

Figure 3 (a, b) UPS spectra of ATS film. (c) Diagram of energy levels (relative to the vacuum level) of ATS light absorber and other functional layers in the ATS thin film solar cell.

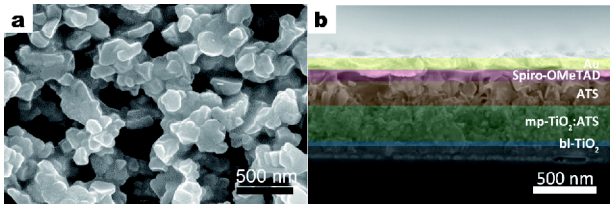

Figure 4 SEM images of (a) ATS nanoparticles and (b) the cross-sectional view of ATS thin film solar cell.

mixed solvent for group α was not enough to fully dissolve SnS_2 and Ag_2S. The precursor concentration for group α was smaller and it leads to a thinner ATS layer. The thinner ATS layer could not afford sufficient light absorption and reduced the J_{SC} of group α. Group γ exhibited a poor performance, because the reaction between mercapto group and amine would increase the viscosity of precursor solution with more TGA. The precursor solution for group γ was too viscous to be spin-coated on the substrate, resulting in the formation of thick and rough ATS films which increased the series resistance and low J_{SC}. The ATS film thickness of group γ may exceed the carrier diffusion length of ATS, which increased charge recombination and decreased the V_{OC} and FF. Fig. 5b shows good photovoltaic performance reproducibility of group α and β, while the poor reproducibility of group γ can be attributed to the inhomogeneity of ATS films. SnS_2 is a binary sulfide light absorber which also has a suitable band gap and an absorption coefficient of more than 10^4 cm^{-1}. The synthesis of SnS_2 demands high cost vacuum techniques and the SnS_2 solar cell based on precipitation chemical method still presented a limited PCE of 0.0023% [39]. Different from SnS_2, ATS-based devices shows a reproducible PCE of about 0.25% after optimization.

The *J*–*V* curves and incident photon-to-electron conversion efficiency (IPCE) of optimized ATS-based device were investigated to reveal the main reason of the limited photovoltaic performance of ATS-based solar cells (Fig. 6a, b). The optimized ATS-based device shows a PCE of 0.255% under AM 1.5G and the *J*–*V* curve measured in the dark confirmed the validity of the photovoltaic behavior. The integrated J_{SC} from the IPCE spectrum is 0.813 mA cm^{-2}. The IPCE can be expressed as follows: IPCE=LHE×ϕ_{inj}×η_C, where LHE stands for the light harvesting efficiency, ϕ_{inj} is electron injection efficiency and η_C is charge collection efficiency. By combining the IPCE and LHE (Fig. 6c), the J_{SC} of the ATS-based device is surrendered by the low ϕ_{inj} and η_C. The steady-state photoluminescence (PL) spectra in Fig. S4 reveal insufficient charge injection efficiencies between ATS and the charge transport layers. As a consequence, the insufficient charge injection efficiency and charge collection efficiency limit the performance of the ATS-based device. The AFM image in Fig. S3 indicates that there were some

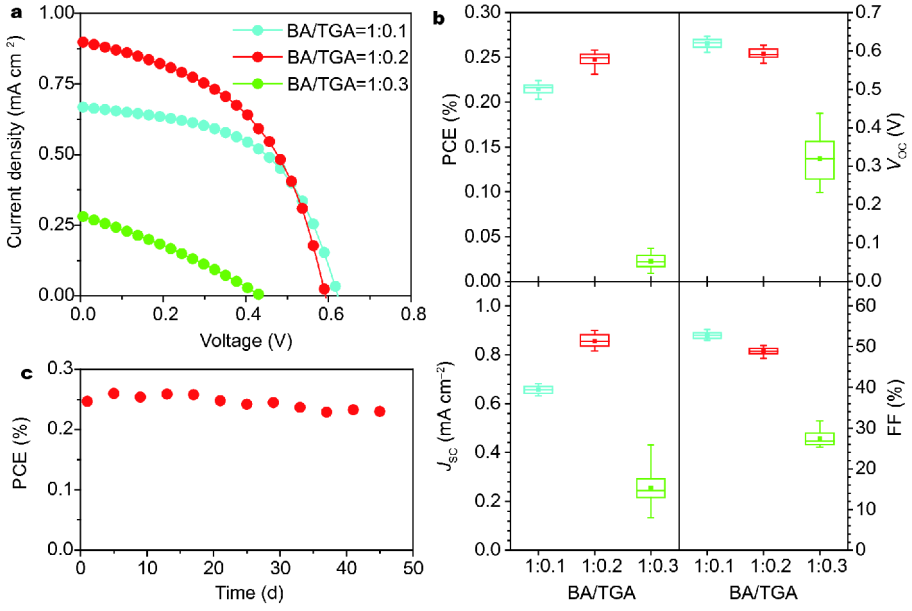

Figure 5 (a) *J*–*V* curves of typical ATS-based devices made from different volume ratio of BA/TGA mixed solvent, obtained under AM 1.5 illumination, 100 ms dwell time. (b) PCE, V_{OC}, J_{SC} and FF *versus* volume ratio of BA/TGA mixed solvent. Each group contains 16 samples. (c) Stability test of PCE degradation of ATS-based unsealed solar cell, the device was tested and stored in ambient conditions.

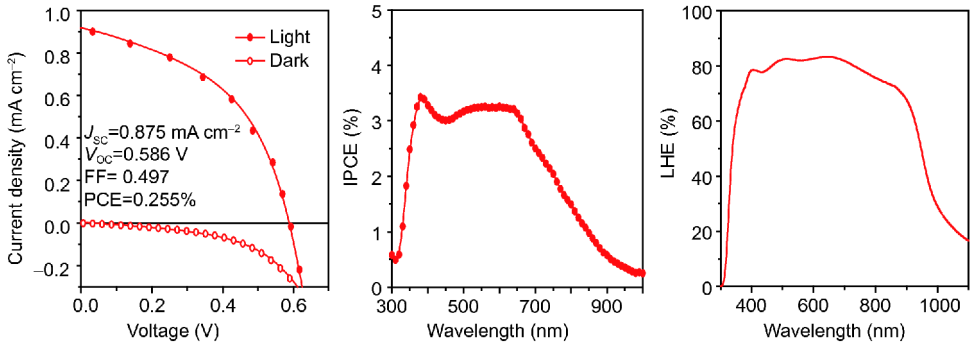

Figure 6 (a) *J*–*V* curves of an optimized ATS-based device obtained under AM 1.5G and in the dark, and the corresponding (b) IPCE spectrum, (c) LHE spectrum.

voids between the crystals in the ATS film. The charge transport materials can fill in these voids and form a structure similar to bulk heterojunction. But different from the bulk heterojunction of organic solar cell which is formed by one mixed solution, the charge transport materials and light absorption material of ATS-based devices were deposited separately. Thus, the interface between ATS and charge transport layers might have some trap states and recombination centers. These traps will hinder the charge injection between ATS and charge transport layers and highly increase charge recombination at the interface. These issues limit the charge injection and collection efficiency and finally resulted in the decrease of J_{SC}.

The long-term stability, over 1,000 h, of ATS-based unsealed device is shown in Fig. 5c. The devices were tested and stored in ambient conditions for 45 days with humidity of 20%–50% at 15–25°C. The devices were stored in the dark. In the first 20 days, the device exhibited an excellent retention of PCE. Without encapsulation, 90% of the initial PCE was still retained after 45 days in ambient conditions. We attributed the little PCE degradation to the metal-migration between back contact Au and organic HTM spiro-OMeTAD [40]. Despite this slight degradation, the ATS-based thin film solar cell still exhibited a good performance in the long-term stability test. By comparing with the instability of the perovskite solar cells which was caused by the chemical instability of perovskite light absorption material, the long term stability of ATS-based devices should be mainly attributed to the remarkable chemical stability of ATS.

CONCLUSIONS

In summary, ATS was synthesized by a novel facile solution-processed method and applied as light absorber in thin film solar cells. ATS has a great chemical stability and is environmentally friendly without toxic element. In our research, well crystallized ATS films were obtained by employing specific BA/TGA mixed solvent in the solution-processed method. The synthesized ATS has a narrow band gap of 1.26 eV which is close to the ideal band gap and a wide absorption wavelength. By considering the CBE and VBE of ATS film, a structure that can be beneficial for the charge separation was employed in ATS-based thin film solar cells: FTO/blocking-TiO_2/mp-TiO_2:ATS/ATS/spiro-OMeTAD/Au. After a series of optimization, ATS-based device with a reproducible PCE of about 0.25% can be achieved. About 90% of the initial PCE of unsealed ATS-based solar cell was remained after 45 days. This research can provide a novel perspective toward the application and investigation of light absorber in thin film solar cells. Just as $CsPbI_3$ based solar cell which exhibited a poor initial PCE of 0.09% [41] and then was improved with a PCE up to 10% in just two years [42], ATS-based thin film solar cell can positively be a competitive candidate in the photovoltaic field in the near future.

Received 17 February 2018; accepted 4 April 2018; published online 11 May 2018

1 Service RF. Perovskite solar cells gear up to go commercial. Science, 2016, 354: 1214–1215
2 Kramer IJ, Sargent EH. The architecture of colloidal quantum dot solar cells: materials to devices. Chem Rev, 2014, 114: 863–882
3 Bernechea M, Miller NC, Xercavins G, *et al.* Solution-processed solar cells based on environmentally friendly $AgBiS_2$ nanocrystals. Nat Photonics, 2016, 10: 521–525
4 Sinsermsuksakul P, Sun L, Lee SW, *et al.* Overcoming efficiency limitations of SnS-based solar cells. Adv Energy Mater, 2014, 4: 1400496
5 Espindola-Rodriguez M, Sylla D, Sánchez Y, *et al.* Bifacial kesterite

solar cells on FTO substrates. ACS Sustain Chem Eng, 2017, 5: 11516–11524
6 Steinmann V, Jaramillo R, Hartman K, *et al.* 3.88% efficient tin sulfide solar cells using congruent thermal evaporation. Adv Mater, 2014, 26: 7488–7492
7 Guo Y, Lei H, Li B, *et al.* Improved performance in Ag_2S/P3HT hybrid solar cells with a solution processed SnO_2 electron transport layer. RSC Adv, 2016, 6: 77701–77708
8 Kojima A, Teshima K, Shirai Y, *et al.* Organometal halide perovskites as visible-light sensitizers for photovoltaic cells. J Am Chem Soc, 2009, 131: 6050–6051
9 Chuang CHM, Brown PR, Bulović V, *et al.* Improved performance and stability in quantum dot solar cells through band alignment engineering. Nat Mater, 2014, 13: 796–801
10 Pan Z, Zhao K, Wang J, *et al.* Near infrared absorption of $CdSe_xTe_{1-x}$ alloyed quantum dot sensitized solar cells with more than 6% efficiency and high stability. ACS Nano, 2013, 7: 5215–5222
11 Panthani MG, Kurley JM, Crisp RW, *et al.* High efficiency solution processed sintered CdTe nanocrystal solar cells: the role of interfaces. Nano Lett, 2014, 14: 670–675
12 Romanyuk YE, Hagendorfer H, Stücheli P, *et al.* All solution-processed chalcogenide solar cells—from single functional layers towards a 13.8% efficient CIGS device. Adv Funct Mater, 2015, 25: 12–27
13 Major JD, Treharne RE, Phillips LJ, *et al.* A low-cost non-toxic post-growth activation step for CdTe solar cells. Nature, 2014, 511: 334–337
14 Lee MM, Teuscher J, Miyasaka T, *et al.* Efficient hybrid solar cells based on meso-superstructured organometal halide perovskites. Science, 2012, 338: 643–647
15 Chen H, Pan X, Liu W, *et al.* Efficient panchromatic inorganic–organic heterojunction solar cells with consecutive charge transport tunnels in hole transport material. Chem Commun, 2013, 49: 7277–7279
16 Li X, Bi D, Yi C, *et al.* A vacuum flash-assisted solution process for high-efficiency large-area perovskite solar cells. Science, 2016, 353: 58–62
17 Zhou H, Chen Q, Li G, *et al.* Interface engineering of highly efficient perovskite solar cells. Science, 2014, 345: 542–546
18 Huang F, Dkhissi Y, Huang W, *et al.* Gas-assisted preparation of lead iodide perovskite films consisting of a monolayer of single crystalline grains for high efficiency planar solar cells. Nano Energy, 2014, 10: 10–18
19 Ding X, Ren Y, Wu Y, *et al.* Sequential deposition method fabricating carbonbased fully-inorganic perovskite solar cells. Sci China Mater, 2017, 61: 73–79
20 Hou Y, Du X, Scheiner S, *et al.* A generic interface to reduce the efficiency-stability-cost gap of perovskite solar cells. Science, 2017, 358: 1192–1197
21 Zuo C, Bolink HJ, Han H, *et al.* Advances in perovskite solar cells. Adv Sci, 2016, 3: 1500324
22 Grätzel M. The light and shade of perovskite solar cells. Nat Mater, 2014, 13: 838–842
23 Chen H, Hou Y, Halbig CE, *et al.* Extending the environmental lifetime of unpackaged perovskite solar cells through interfacial design. J Mater Chem A, 2016, 4: 11604–11610
24 Zuo C, Ding L. Lead-free perovskite materials $(NH_4)_3Sb_2I_xBr_{9-x}$. Angew Chem Int Ed, 2017, 56: 6528–6532
25 Bai H, Shen T, Wang S, *et al.* Controlled growth of Cu_3Se_2 nanosheets array counter electrode for quantum dots sensitized solar cell through ion exchange. Sci China Mater, 2017, 60: 637–645
26 Zhao J, Liu Z, Tang H, *et al.* Enhanced performance of solar cells *via* anchoring $CuGaS_2$ quantum dots. Sci China Mater, 2017, 60: 829–838
27 Volonakis G, Haghighirad AA, Milot RL, *et al.* $Cs_2InAgCl_6$: a new lead-free halide double perovskite with direct band gap. J Phys Chem Lett, 2017, 8: 772–778
28 Polman A, Knight M, Garnett EC, *et al.* Photovoltaic materials: Present efficiencies and future challenges. Science, 2016, 352: aad4424
29 Park NG. Perovskite solar cells: an emerging photovoltaic technology. Mater Today, 2015, 18: 65–72
30 Kameyama T, Fujita S, Furusawa H, *et al.* Size-controlled synthesis of Ag_8SnS_6 nanocrystals for efficient photoenergy conversion systems driven by visible and near-IR lights. Part Part Syst Charact, 2014, 31: 1122–1126
31 Yeh LY, Cheng KW. Preparation of chemical bath synthesized ternary Ag–Sn–S thin films as the photoelectrodes in photoelectrochemical cell. J Power Sources, 2015, 275: 750–759
32 Shambharkar BH, Chowdhury AP. Ethylene glycol mediated synthesis of Ag_8SnS_6 nanoparticles and their exploitation in the degradation of eosin yellow and brilliant green. RSC Adv, 2016, 6: 10513–10519
33 Cheng KW, Tsai WT, Wu YH. Photo-enhanced salt-water splitting using orthorhombic Ag_8SnS_6 photoelectrodes in photoelectrochemical cells. J Power Sources, 2016, 317: 81–92
34 Hu WQ, Shi YF, Wu LM. Synthesis and shape control of Ag_8SnS_6 submicropyramids with high surface energy. Cryst Growth Des, 2012, 12: 3458–3464
35 Zhao W, Wang G, Tian Q, *et al.* Fabrication of $Cu_2ZnSn(S,Se)_4$ solar cells *via* an ethanol-based sol–gel route using SnS_2 as Sn source. ACS Appl Mater Interfaces, 2014, 6: 12650–12655
36 Webber DH, Brutchey RL. Alkahest for V_2VI_3 chalcogenides: dissolution of nine bulk semiconductors in a diamine-dithiol solvent mixture. J Am Chem Soc, 2013, 135: 15722–15725
37 Abdullah Almessiere M, Al-Otaibi AL, Assaker IB, *et al.* Electrodeposited and characterization of Ag–Sn–S semiconductor thin films. Mater Sci Semicond Proc, 2015, 40: 267–275
38 Hagfeldt A, Grätzel M. Light-induced redox reactions in nanocrystalline systems. Chem Rev, 1995, 95: 49–68
39 Khot KV, Ghanwat VB, Bagade CS, *et al.* Synthesis of SnS_2 thin film *via* non vacuum arrested precipitation technique for solar cell application. Mater Lett, 2016, 180: 23–26
40 Domanski K, Correa-Baena JP, Mine N, *et al.* Not all that glitters is gold: metal-migration-induced degradation in perovskite solar cells. ACS Nano, 2016, 10: 6306–6314
41 Choi H, Jeong J, Kim HB, *et al.* Cesium-doped methylammonium lead iodide perovskite light absorber for hybrid solar cells. Nano Energy, 2014, 7: 80–85
42 Swarnkar A, Marshall AR, Sanehira EM, *et al.* Quantum dot-induced phase stabilization of α-$CsPbI_3$ perovskite for high-efficiency photovoltaics. Science, 2016, 354: 92–95

Acknowledgements This work was financially supported by the National High Technology Research and Development Program of China (2015AA050602), the Project of Science and Technology Service (STS) Network Initiative, Chinese Academy of Sciences (KFJ-SW-STS-152).

Author contributions Zhu L conducted the main experiments and

wrote this manuscript. Pan X directly guided this research including the designing, modifying and optimizing work related to this manuscript. Dai S supervised the projects and carefully reviewed and modified this manuscript. Xu Y, Zheng H, Liu G, Xu X provided help in the fabrication of devices and methods of characterization. All authors contributed to the general discussion about this work.

Conflict of interest The authors declare no competing financial interests.

Supplementary information Supporting data are available in the online version of the paper.

Liangzheng Zhu received his Bachelor degree from the East China University of Science and Technology in 2012. He is currently pursuing his PhD degree in the University of Science and Technology of China. His research interests mainly focus on thin film solar cells.

Xu Pan received his PhD degree from the Chinese Academy of Sciences in 2007. He joined Hefei Institutes of Physical Science, Chinese Academy of Sciences and was promoted to full professor in 2013. Now his research interests focus on the new generation solar cells, including dye-sensitized solar cells and perovskite solar cells, etc.

Songyuan Dai is a professor and Dean of the School of Renewable Energy, North China Electric Power University. He obtained his BSc degree in physics from Anhui Normal University in 1987, and MSc and PhD degrees in plasma physics from the Institute of Plasma Physics, Chinese Academy of Sciences in 1991 and 2001. His research interests mainly focus on next-generation solar cells including dye-sensitized solar cells, quantum dot solar cells, perovskite solar cells, etc.

温和溶液法制备三元硫化物Ag_8SnS_6作为吸光材料在薄膜太阳电池中的应用

朱梁正[1,2], 徐亚峰[1,2], 郑海英[1,2], 刘国震[1,2], 徐笑笑[1,2], 潘旭[1*], 戴松元[3*]

摘要 吸光材料是薄膜太阳电池进一步应用的重要因素. 三元硫化物Ag_8SnS_6 (ATS)拥有诸多优秀的光电性质. 然而, 关于ATS在吸光材料方面的应用鲜有报道. 因此, 本文通过使用一种退火温度低于250°C的温和溶液法制备ATS吸光材料并将其应用于薄膜太阳电池. 在优化之后, 基于ATS的薄膜太阳电池展现出了具有潜力的光伏性能以及可再现的0.25%光电转化效率. 更重要的是, 基于ATS的器件展现出了卓越的长期稳定性, 在超过1000小时的老化测试后器件仍然还有90%的初始效率. 本研究不仅揭示了含量丰富、低毒且化学性质稳定的ATS作为吸光材料的潜力, 也为薄膜太阳电池中新型吸光材料的研究提供了全新的视角.

